

Learning to Select Camera Views: Efficient Multiview Understanding at Few Glances

Yunzhong Hou Stephen Gould Liang Zheng
Australian National University
{firstname.lastname}@anu.edu.au

Abstract

Multiview camera setups have proven useful in many computer vision applications for reducing ambiguities, mitigating occlusions, and increasing field-of-view coverage. However, the high computational cost associated with multiple views poses a significant challenge for end devices with limited computational resources. To address this issue, we propose a view selection approach that analyzes the target object or scenario from given views and selects the next best view for processing. Our approach features a reinforcement learning based camera selection module, MVSelect, that not only selects views but also facilitates joint training with the task network. Experimental results on multiview classification and detection tasks show that our approach achieves promising performance while using only 2 or 3 out of N available views, significantly reducing computational costs. Furthermore, analysis on the selected views reveals that certain cameras can be shut off with minimal performance impact, shedding light on future camera layout optimization for multiview systems. Code is available at <https://github.com/hou-yz/MVSelect>.

1. Introduction

Multiple camera views (multiview) are popular in computer vision systems for their ability to address challenges such as occlusions, ambiguities, and limited field-of-view (FoV) coverage. Tasks like classification [38, 30] and detection [5, 17] have shown significant benefits from using multiple cameras (Fig. 1). With reduced hardware cost and easy deployment, real-world products now include more cameras at larger scales. For example, iPhones went from one to three rear lenses [3]; autopilot cars went from two cameras in the ARGO project [29] to eight in Tesla [41]; and future smart cities will also incorporate more cameras [9].

However, the use of multiple cameras comes at a high computational cost, which can be a significant challenge for end devices with limited computational resources, es-

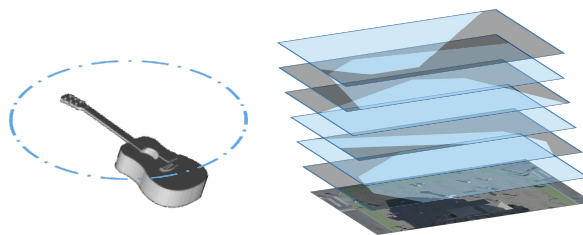


Figure 1: Example of multiview camera setups. **Left:** multiview classification jointly considers multiple camera views to identify the object. Cameras (blue dots) follow a certain layout [46, 20] to provide complementary view-points. **Right:** multiview detection estimates pedestrian occupancy from bird’s-eye-view (bottom colored image). Cameras (blue FoV maps) can be set at different locations [5, 17] to increase FoV coverage and deal with occlusion. For both classification and detection tasks, due to hardware constraints, camera layouts are usually pre-defined.

pecially with higher image resolutions [36, 33] and deeper neural network backbones [15, 8]. Limiting image resolution or using lighter networks [28, 18] are current options to reduce computation, but they may impede the progress in camera sensors or neural network architecture.

To address this challenge, this paper proposes a new approach to efficient multiview understanding by selecting only the most useful views. To identify the best views, this approach leverages camera layouts, which is a key aspect overlooked by existing alternatives. With known camera layouts, networks should be able to infer what each camera view looks like and then choose accordingly, as previous works [20] have shown that networks can associate images with camera poses. Existing work on active vision [1, 11, 7] also indicates that it is possible to smartly select the camera locations and directions for better robot vision. In our problem, for example (see Fig. 2), we might confuse a guitar with a mandolin from the side view. Previous knowledge of the camera layout should inform the system that the front view can clear the ambiguities and should be queried.

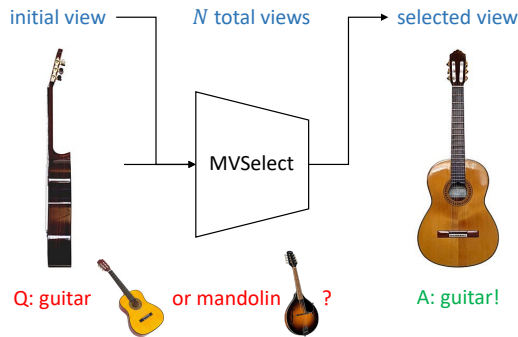


Figure 2: Efficient multiview understanding with two glances. Instead of using all N views at once, a more efficient approach is to first examine one view and then select another view that should resolve ambiguities in the initial glance. In this example, if the initial side view cannot distinguish between a guitar and a mandolin (a round-shaped instrument that may also have a flat back), we can query the front view in the second glance to clarify the ambiguities.

To achieve this goal, this paper proposes a novel view selection module, MVSelect, that chooses the best camera views from any initial view. The proposed module first analyzes the target object or scenario using the given view and then selects the next view that best helps the task (multiview classification or detection) network. To navigate through the non-differentiable parts in view selection, we formulate this interactive process as a reinforcement learning problem [26] that considers the chosen cameras and their visual feedback as state, the next camera to select as action, and the final result from the task network as reward.

On both multiview classification and detection tasks, our experimental results show that MVSelect can provide a good strategy for fixed task networks, while also capable of joint training with the task network for further performance improvements. Specifically, when allowing joint training on both MVSelect and the task network, the resulting system can achieve similar results to using all N cameras, while using only 2 views for classification tasks and 3 views for detection tasks, respectively.

The computational overhead of MVSelect is very small, as it shares the feature extraction backbone with the task network and only has a few learnable layers. For the entire system, the computational cost is roughly proportional to the number of views used, resulting in approximately $2/N$ of the total computation when only 2 views are used, a significant efficiency boost.

The MVSelect policy also enables study on multiview camera layout. In fact, we find that many of the N cameras are rarely chosen and can be shut off for further operational cost improvements, which can serve as a starting point for future study on multiview camera layout.

2. Background

Multiview classification. One effective way for 3D shape recognition is to capture the object in multiple camera views. MVCNN [38] extracts feature vectors from the input views, and then uses max pooling to aggregate across multiple views for classification. Based on MVCNN, many alternative approaches are proposed. Qi *et al.* [30] propose sphere rendering at different volume resolutions. GVCNN [10] investigates hierarchical information between different views by grouping the image features before the final aggregation. RotationNet [20] introduces a multi-task objective by jointly considering classification and camera poses. ViewGCN [44] uses a Graph Convolution Network (GCN) [23] instead of the max pooling layer to aggregate across views. Recently, Hamdi *et al.* [14] propose the MVTN network to estimate the best viewpoints for 3D point cloud models.

Multiview detection. Occlusion is a key problem for object detection, and is by nature very difficult to tackle using only one camera view. To deal with this problem, researchers investigate multiview approaches for pedestrian detection and estimate occupancy from the bird’s-eye-view (BEV). For this task, some methods [12, 32, 47] aggregate single-view detection results. Others [4, 6, 17] find single-view detection results unreliable and instead aggregate the features. Specifically, Hou *et al.* [17] introduce MVDet, a fully convolutional approach that projects feature maps from each camera view to the BEV. Inspired by MVDet, researchers introduce other novel methods. SHOT [37] projects the image feature map at different heights and stacks them together to improve performance. MVDeTr [16] deals with distinct distortion patterns from the projection. Qiu *et al.* [31] investigate data augmentation with simulated occlusion over multiple views.

Camera viewpoint study. Camera viewpoint is an important factor in multiview systems. Previous works on active vision investigate sensor planning, where the pose and settings of vision sensors are determined for robot vision tasks [1, 11, 7]. In multiview classification, RotationNet [20] makes some pioneering work on limited view numbers by taking a random partial set of all N views of the image. MVTN [14] uses the 3D point cloud as initial input and then estimates the best camera layout for multiview classification, but its moving camera assumption is hard to met in real-world systems such as iPhones [3] and Teslas [41]. In multiview detection, Vora *et al.* [42] investigate camera layout generalization by randomly dropping camera views from both training and testing.

Reinforcement learning (RL) directs an agent to interact with the environment in a manner that maximizes cumulative rewards. State $s \in \mathcal{S}$, action $a \in \mathcal{A}$, and reward $r \in \mathcal{R}$ are key concepts to model the interaction between agent and environment. In a certain state s , policy $\pi(a|s)$

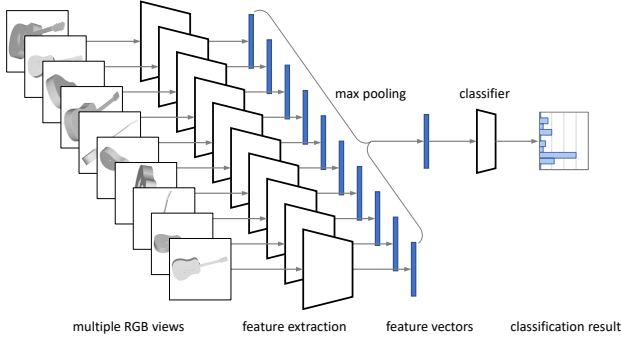


Figure 3: Multiview classification with MVCNN [38].

records the probability for each action, and state value function $V(s)$ estimates the future rewards when following the corresponding policy. To learn the best policy, Q-learning and DQN [27] optimize the action value function $Q(s, a)$, which describes the estimated future return for a specific action a at state s . Policy gradient methods like REINFORCE [45] and PPO [35] directly optimize for the policy $\pi(a|s)$.

Reinforcement learning has been used in many vision tasks. To deal with non-differentiable parts, Schulman *et al.* [34] use RL to estimate loss function’s gradient. Minh *et al.* [26] recognize an image by navigating an agent with a small receptive field. Embodied vision [50, 2] uses RL to navigate an agent to the final destination.

3. Multiview Network Revisit

3.1. Multiview Classification: MVCNN

MVCNN [38] (Fig. 3) is a classic architecture which many multiview classification networks [30, 10, 20, 49, 43, 48, 44, 14] build upon. Given N input images $\mathbf{x}_n, n \in \{1, \dots, N\}$, first, MVCNN uses its feature extractor $f(\cdot)$ to calculate the feature vectors,

$$\mathbf{h}_n = f(\mathbf{x}_n), \quad (1)$$

where the feature vector $\mathbf{h}_n \in \mathbb{R}^D$ is D -dimensional. Secondly, it uses max pooling to aggregate multiple views into an overall feature descriptor $\hat{\mathbf{h}} \in \mathbb{R}^D$,

$$\hat{\mathbf{h}}_d = \max_n \{\mathbf{h}_{n,d}\}, \quad d \in \{1, \dots, D\}, \quad (2)$$

where $\hat{\mathbf{h}}_d$ and $\mathbf{h}_{n,d}$ denote the d dimension of $\hat{\mathbf{h}}$ and \mathbf{h}_n , respectively. Lastly, it applies the output head $g(\cdot)$ as,

$$\hat{\mathbf{y}} = g(\hat{\mathbf{h}}), \quad (3)$$

to produce the classification result $\hat{\mathbf{y}}$.

In training, the original design by Su *et al.* [38] adopts a 2-stage paradigm by first training on individual views and

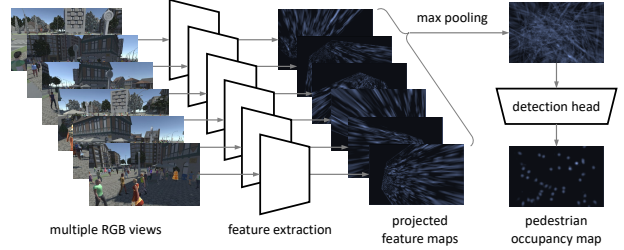


Figure 4: Multiview detection with MVDet [17].

then considering multiple views. In this paper, we skip the first stage and directly train MVCNN on all N views,

$$\mathcal{L}_{\text{MVCNN}} = \mathcal{L}_{\text{CE}}(\hat{\mathbf{y}}, \mathbf{y}), \quad (4)$$

where $\mathcal{L}_{\text{CE}}(\cdot, \cdot)$ denotes the cross-entropy loss and \mathbf{y} denotes the ground truth one-hot label.

3.2. Multiview Detection: MVDet

MVDet [17] (Fig. 4) is a multiview detection architecture that estimates human occupancy in bird’s-eye-view (BEV). Its feature projection and anchor-free design have been adopted by many recent works [16, 37, 42, 31, 13, 25, 19]. Given input images $\mathbf{x}_n, n \in \{1, \dots, N\}$, MVDet first extracts D -channel feature maps for each view and uses perspective transformation to project the camera views to the BEV. These operations can be jointly considered as the BEV feature extraction step under Eq. 1, with the exception that $\mathbf{h}_n \in \mathbb{R}^{D \times H \times W}$ now denotes the D -channel feature map for the BEV scenario of shape $H \times W$. Secondly, for multiview aggregation, instead of the concatenation in the original design, we choose element-wise max pooling in Eq. 2, producing the overall feature description $\hat{\mathbf{h}} \in \mathbb{R}^{D \times H \times W}$ that fits arbitrary numbers of views. Lastly, we apply the output head as Eq. 3 to generate a heatmap $\hat{\mathbf{y}} \in [0, 1]^{H \times W}$ that indicates the likelihood of human occupancy in each BEV location.

The loss we used for MVDet training can be written as,

$$\mathcal{L}_{\text{MVDet}} = \mathcal{L}_{\text{BEV}}(\hat{\mathbf{y}}, \mathbf{y}) + \frac{1}{N} \sum_{n=1}^N \mathcal{L}_n, \quad (5)$$

where $\mathcal{L}_{\text{BEV}}(\cdot, \cdot)$ denotes BEV output loss; $\mathbf{y} \in \{0, 1\}^{H \times W}$ denotes binary ground truth map; and \mathcal{L}_n denotes the auxiliary per-view loss with 2D bounding boxes.

4. Efficient Multiview Understanding

In a multiview system with N views, our efficient approach uses a total of $T < N$ camera views $a_t \in \{1, \dots, N\}, t \in \{1, \dots, T\}$ for multiview understanding. To achieve this, we propose a view selection module, MVSelect, denoted as $d(\cdot)$, which sequentially selects camera

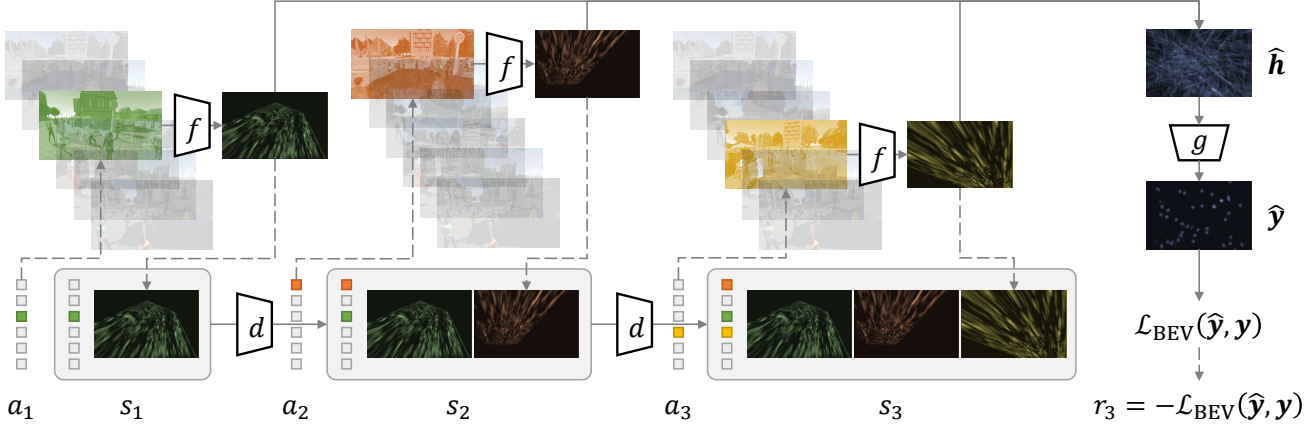


Figure 5: Efficient multiview understanding with a total of $T = 3$ glances. Solid lines indicate the network forward pass and dashed lines indicate the interaction between *agent* (MVSelect) and *environment* (multiview system). The approach starts with a random **initial view** a_1 , and the feature extractor $f(\cdot)$ is used to compute its feature \mathbf{h}_{a_1} (Eq. 1). The *state* for this initial time step is recorded as s_1 (Eq. 6). Next, the proposed MVSelect module $d(\cdot)$ is used to choose a **second view** a_2 , which is the *action* for state s_1 . The feature representation \mathbf{h}_{a_2} for this second view is computed, and the state for the two views is updated as s_2 . Then, by repeating the last step, a **third view** a_3 is chosen based on state s_2 . The feature representation \mathbf{h}_{a_3} and the state s_3 are also updated accordingly. Finally, three views are aggregated into an **overall descriptor** $\hat{\mathbf{h}}$ (Eq. 2), and the task network output $\hat{\mathbf{y}}$ is calculated using the output head $g(\cdot)$ (Eq. 3). For multiview detection, the final *reward* $r_3 = -\mathcal{L}_{\text{BEV}}(\hat{\mathbf{y}}, \mathbf{y})$ is set as the negative of the BEV loss (Eq. 7), and all other rewards are assigned as zero.

views. Starting from a random initial view a_1 , MVSelect chooses the remaining $T - 1$ cameras by observing the target object or scene from existing views a_1, \dots, a_t at each time step t and deciding which camera view a_{t+1} to select next. The resulting T views should give the task network high classification or detection performance.

Once T camera views have been gathered, we aggregate them into an overall description $\hat{\mathbf{h}}$ using Eq. 2, and calculate the final output $\hat{\mathbf{y}}$ using Eq. 3. Figure 5 gives an overview of the proposed efficient multiview approach.

4.1. Problem Formulation

We can frame this interactive process as a reinforcement learning problem, where MVSelect is the *agent* and the multiview system is the *environment*.

State. For a time step t , we record the chosen camera views a_1, \dots, a_t and the observations $\mathbf{h}_{a_1}, \dots, \mathbf{h}_{a_t}$ as state s_t . We use the extracted features to represent the observations rather than the RGB camera views $\mathbf{x}_{a_1}, \dots, \mathbf{x}_{a_t}$ to reduce dimensionality and maximize efficiency, since these features will be used in the task network later (Eq. 2).

Mathematically, we formulate the state s_t as follows,

$$\begin{aligned}
 s_t &= \langle s_t^{\text{cam}}, s_t^{\text{obs}} \rangle, \\
 s_t^{\text{cam}} &= \sum_{\tau=1}^t \text{onehot}(a_\tau), \\
 s_{t,d}^{\text{obs}} &= \max_{\tau=1}^t \{ \mathbf{h}_{a_\tau, d} \}, \quad d \in \{1, \dots, D\},
 \end{aligned} \tag{6}$$

where $\text{onehot}(\cdot)$ is the one-hot function over N cameras. This representation reflects both chosen cameras $s_t^{\text{cam}} \in \mathbb{R}^N$ and their observations $s_t^{\text{obs}} \in \mathbb{R}^D$, and maintains the same dimensionality across different time steps. The observation part s_t^{obs} also matches the overall representation in Eq. 2.

Action. For state $s_t, t \in \{1, \dots, T - 1\}$, MVSelect takes the $t + 1$ camera view a_{t+1} as action.

Reward. Upon taking action a_{t+1} , the system receives reward r_{t+1} and transitions into the next state s_{t+1} . To achieve high task network performance, we consider the following as reward,

$$\begin{aligned}
 r_t &= 0, \quad t \in \{1, \dots, T - 1\}, \\
 r_T^{\text{MVCNN}} &= \mathbb{1}(\hat{\mathbf{y}} = \mathbf{y}), \quad r_T^{\text{MVDet}} = -\mathcal{L}_{\text{BEV}}(\hat{\mathbf{y}}, \mathbf{y}),
 \end{aligned} \tag{7}$$

where $\mathbb{1}(\cdot)$ denotes the binary indicator function. For the last time step, we use classification accuracy or the inverse of the BEV loss (Eq. 5) as reward r_T for the two problems, respectively. For all other time steps, we set r_t as zero.

4.2. MVSelect Architecture

As shown in Fig. 6, we design MVSelect architecture $d(\cdot)$ with two branches. The first branch expands the camera selection result $s_t^{\text{cam}} \in \mathbb{R}^N$ into D -dimensional learnable camera embeddings, and then sums over the selected embeddings to formulate a hidden vector. The second branch processes the observation $s_t^{\text{obs}} \in \mathbb{R}^D$, and converts that into another hidden vector. By combining the two hidden vectors, MVSelect outputs the action-value $Q(s, a)$,

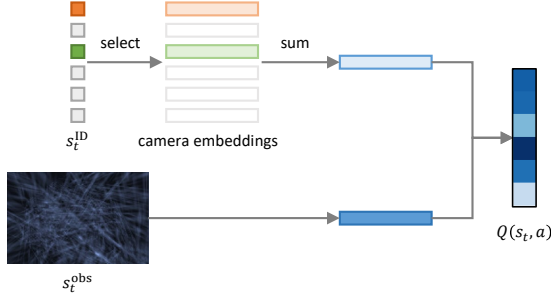


Figure 6: MVSelect architecture.

which measures the expected cumulative rewards for taking an action a in a given state s .

During testing, MVSelect outputs the next action as,

$$a_{t+1} = \arg \max_a Q(s_t, a),$$

which maximizes the expected cumulative rewards.

4.3. Training Scheme

We adopt Q-learning [39] for training MVSelect. Specifically, action-value function $Q(\cdot, \cdot)$ should estimate the cumulative future rewards after taking action a_{t+1} at state s_t ,

$$Q(s_t, a_{t+1}) = \mathbb{E} \left(\sum_{\tau=t+1}^T \gamma^{\tau-t-1} r_\tau \right),$$

where $\mathbb{E}(\cdot)$ denotes the expectation, and $\gamma \in [0, 1]$ denotes the discount factor. We take the temporal difference (TD) [39] target as supervision for the action value,

$$q_t = \begin{cases} r_{t+1} + \gamma \max_a Q(s_{t+1}, a), & \text{if } t < T - 1 \\ r_T, & \text{otherwise} \end{cases}, \quad (8)$$

and calculate the loss using the L_2 distance,

$$\mathcal{L}_{\text{RL}} = \sum_{t=1}^{T-1} \mathcal{L}_{\text{MSE}}(Q(s_t, a_{t+1}), q_t), \quad (9)$$

where the next action a_{t+1} is chosen using ϵ -greedy for exploration-exploitation trade offs (see Algorithm 1).

In joint training, the task network takes supervision from the task loss $\mathcal{L}_{\text{task}}$ (Eq. 4 and Eq. 5), and the selection module takes supervision from the RL loss \mathcal{L}_{RL} (Eq. 9). We demonstrate this process step-by-step in Algorithm 1.

5. Experiments

5.1. Experiment Settings

Datasets. We verify the performance of the proposed approach on multiview classification and detection tasks.

Algorithm 1 Joint training of MVSelect and task network.

- 1: **input:** camera views $x_n, n \in \{1, \dots, N\}$, ground truth label y , random initial view a_1 , number of total views T , ϵ , γ .
 - 2: initialize the total loss $\mathcal{L}_{\text{total}} = 0$;
 - 3: **for** $t \in \{1, \dots, T - 1\}$ **do**
 - 4: select and apply the next action using ϵ -greedy: with probability ϵ adopt a random action, or else choose the action with highest value $a_{t+1} = \arg \max_a Q(s_t, a)$;
 - 5: observe next state s_{t+1} (Eq. 6) and reward r_{t+1} (Eq. 7);
 - 6: calculate the TD [39] target q_t (Eq. 8) and update RL loss $\mathcal{L}_{\text{total}} = \mathcal{L}_{\text{total}} + \mathcal{L}_{\text{RL}}$ (Eq. 9);
 - 7: **end for**
 - 8: calculate the task loss $\mathcal{L}_{\text{task}}$ (Eq. 4 and Eq. 5);
 - 9: optimize for the total loss $\mathcal{L}_{\text{total}} = \mathcal{L}_{\text{total}} + \mathcal{L}_{\text{task}}$;
 - 10: **update:** task network $f(\cdot)$ and $g(\cdot)$, and MVSelect $d(\cdot)$.
-

ModelNet40 is a subset of 3D CAD models in ModelNet [46]. It includes 40 categories of synthetic 3D objects with 9,843 training models and 2,468 test models. For multiview classification experiments, we use two different configurations: the *12-view* circular configuration from MVCNN [38] and the *20-view* dodecahedral configuration from RotationNet [20].

Wildtrack [5] is a real-world multiview detection dataset with 7 camera views covering a 12×36 square meter area, which is represented as a 480×1440 grid from BEV. It contains 360 frames for training and 40 frames for testing.

MultiviewX [17] is a synthetic multiview detection dataset created using the Unity [40] engine. It has 6 cameras with higher pedestrian density than Wildtrack. It focuses on a 16×25 square meter area, which is discretized into 640×1000 BEV grid. Like Wildtrack, MultiviewX also contains 360 training frames and 40 testing frames.

Evaluation metrics. For multiview classification, we follow previous methods [30, 20, 44, 49, 48, 14] and report instance-averaged accuracy as the primary indicator.

Regarding multiview detection, we report the following metrics: multi-object detection accuracy (MODA), multi-object detection precision (MODP), precision, and recall [21]. During evaluation, we first compute false positives (FP), false negatives (FN), and true positives (TP), and then use them to calculate the metrics. Specifically, MODA is calculated as $1 - \frac{\text{FP} + \text{FN}}{\text{GT}}$, where GT is the number of ground truth pedestrians. MODP is calculated as $\frac{\sum 1 - \text{dist}(\text{dist} < \text{thres}) / \text{thres}}{\text{TP}}$, where dist is the distance from the estimated pedestrian location to its ground truth and thres is the threshold of 0.5 meters. MODP indicates the BEV localization accuracy. Precision and recall are calculated as $\frac{\text{TP}}{\text{TP} + \text{FP}}$ and $\frac{\text{TP}}{\text{GT}}$, respectively.

All metrics are reported in percentages.

Implementation details. For multiview classification, we input images of size 224×224 to the MVCNN model. For multiview detection, we use a resolution of 720×1280

	ModelNet40 [46]			Wildtrack [5]				MultiviewX [17]			
	12 views	20 views		MODA	MODP	prec.	recall	MODA	MODP	prec.	recall
MVCNN [38]	90.1	92.0	RCNN & cluster [47]	11.3	18.4	68	43	18.7	46.4	63.5	43.9
GVCNN [10]	92.6	-	POM-CNN [12]	23.2	30.5	75	55	-	-	-	-
MHBN [49]	93.4	-	DeepMCD [6]	67.8	64.2	85	82	70	73	85.7	83.3
RotationNet [20]	-	94.7	Deep-Occlusion [4]	74.1	53.8	95	80	75.2	54.7	97.8	80.2
RelationNet [48]	94.3	97.3	MVDet [17]	88.2	75.7	94.7	93.6	83.9	79.6	96.8	86.7
ViewGCN [44]	-	97.6	SHOT [37]	90.2	76.5	96.1	94.0	88.3	82.0	96.6	91.5
MVTN* [14]	93.8	93.5	MVDeTr [16]	91.5	82.1	97.4	94.0	93.7	91.3	99.5	94.2
MVCNN (ours)	94.5	96.5	MVDet (ours)	90.0	80.9	95.4	94.5	93.0	90.3	98.7	94.4

Table 1: Performance comparison with state-of-the-art multiview classification and multiview detection methods. Results are averaged from 5 runs. * indicates that the camera poses are dynamically chosen and do not follow a pre-defined layout.

MVCNN training	view selection	ModelNet40	
		12 views	20 views
from scratch	N/A	94.5	96.5
fixed	random selection	71.5	48.1
fixed	dataset-lvl oracle	85.2	69.9
fixed	instance-lvl oracle	96.5	98.1
fixed	MVSelect	88.2	79.6
joint training	MVSelect	94.3	94.4

Table 2: Evaluation of MVSelect on multiview classification. All view selection results use a total of $T = 2$ views.

for input images with view-coherent data augmentation [16], and downsample the BEV grid by a factor of 4. In terms of architecture, we use ResNet-18 [15] as feature extractor $f(\cdot)$ for both tasks.

We train all networks for 10 epochs using the Adam optimizer [22]. We use learning rates of 5×10^{-5} and 5×10^{-4} , with batch sizes of 8 and 1 for MVCNN and MVDet, respectively. The MVSelect module is trained using a learning rate of 1×10^{-4} . For joint training, we decrease the learning rate for the task network to $1/5$ of its original value.

Regarding hyperparameters, we set the future reward discount factor $\gamma = 0.99$, and the exploration ratio ϵ to gradually decrease from 0.95 to 0.05 during training.

All experiments are conducted on a single RTX-3090 GPU and averaged across 5 repetitive runs.

5.2. Evaluation of Task Networks

In Table 1, we compare our implementations of MVCNN [38] and MVDet [17] with their original implementations and state-of-the-art methods. On 3 datasets and 4 settings, our implementations outperform the original implementations and achieve competitive results. Although our focus is not on improving these classic architectures, the results indicate that they can still serve as strong baselines.

Experimental setups. To demonstrate the full potential of MVSelect, we experiment under two settings.

First, we fix the task network and only train the view selection module. Our goal is to show that the view selec-

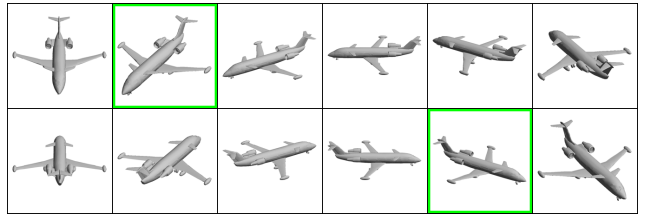


Figure 7: Example of selected views on ModelNet40 [46].

tion results outperform random selection. We also compare the performance of two oracles: for a certain initial view, 1) choosing the overall best-performing camera for all instances in the dataset (*dataset-level oracle*) and 2) choosing specifically for each instance (*instance-level oracle*). The former reflects the upper bound of performance achievable by human-designed heuristics, and the latter represents the theoretical performance ceiling when keeping the task network fixed.

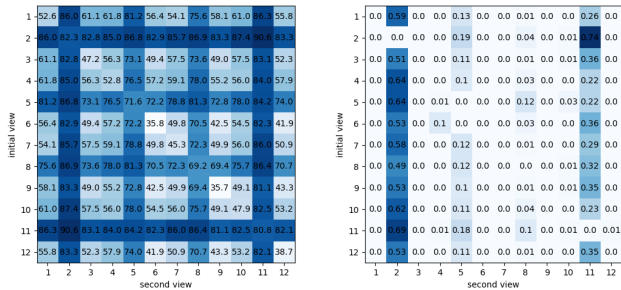
Second, we jointly train the proposed view selection module with the task networks to fully exploit MVSelect. For this experiment, our goal is to achieve the highest possible performance using T views.

If not specified, we use a total of $T = 2$ views for multiview classification and $T = 3$ views for detection.

Results and analysis. In Table 2 and Table 3, we report the view selection results, which are averaged using all N views as the initial view.

For **multiview classification**, as shown in Table 2, randomly selecting two views cannot achieve competitive results. Specifically, We found that when more views are provided, MVCNN [38] tends to only activate on the high-confidence views, resulting in worse performance on the 20-view setup than the 12-view setup.

The proposed view selection module, on the other hand, can choose the supplementary view very effectively. On ModelNet40 dataset [46], MVSelect with fixed MVCNN outperforms the random selection baseline by 16.7% and 31.5% on the 12-view and 20-view setups, respectively. Compared to dataset-level oracles (same policy for all in-



(a) Classification accuracy

(b) MVSelect policy

Figure 8: Multiview classification with $T = 2$ views on the 12-view setup [38] of ModelNet40 [46]. The task network is fixed once trained. **Left:** test set accuracy of using two views. **Right:** MVSelect policy for the test set.

stances with the same initial camera), MVSelect also turns out to be advantageous by 3.0% and 9.7% for the two settings. This verifies that MVSelect can take the target object into consideration (see Fig. 2) and select different cameras for different instances under the same initial camera.

When we allow joint training for both MVSelect and the task network, we witness large improvements compared to keeping MVCNN fixed. In fact, on two settings, the results are only 0.2% and 2.1% behind compared to the full N -view system. Overall, we believe that MVSelect and its joint training capabilities enable us to consider only 2 of the 12 or 20 views without major performance drawbacks.

We demonstrate an example of the selected views in Fig. 7, and the MVSelect policy in Fig. 8.

For **multiview detection**, we report view selection results in Table 3. Since the target scenarios are not fully captured by any individual camera, randomly selecting $T = 3$ cameras does not yield satisfactory results. In addition, we observe that the instance-level oracle remains relatively low compared to that of multiview classification tasks (see Table 2). This is likely due to the target scenarios not being fully captured by any single view, and the multiview detection network needs multiple views to collaborate with each other for optimal results.

In this scenario, we find that MVSelect with a fixed task network can outperform random selection, by 5.1% MODA on Wildtrack [5] and 2.5% MODA on MultiviewX [17]. Although the raw improvements are not as substantial as those in multiview classification, they are **statistically highly significant** (p-value < 0.001). Compared to the dataset-level oracles, we find the MVSelect policy lose its edge. In fact, we find that for multiview detection, MVSelect tends to select the same camera for a given initial view, since it is *not* aware of the situation outside of the FoV coverage. As a result, it cannot choose cameras based on *uncovered* areas in different frames. Without this instance-aware advantage,

MVDet training	view selection	Wildtrack	MultiviewX
from scratch	N/A	90.0	93.0
fixed	random selection	74.9	76.2
fixed	dataset-lvl oracle	82.5	80.2
fixed	instance-lvl oracle	87.4	82.3
fixed	MVSelect	80.0	78.7
joint training	MVSelect	88.6	88.1

Table 3: Evaluation of MVSelect on multiview detection. We report MODA since it accounts for both precision and recall, plus MODP is not affected too much. All view selection results use a total of $T = 3$ views.



Figure 9: Example of selected views on Wildtrack [5].

the fixed camera policy learned during training (MVSelect) cannot outperform the dataset-level oracle, whose policy is computed on the test set.

On the positive side, joint training with MVDet once again leads to substantial performance improvements over keeping the task network fixed. In fact, the results even exceed the instance-level oracle for fixed task networks. This phenomenon demonstrates the high level of camera collaboration in normal N -camera training protocols, and show that joint training improves task network generalization. Using $T = 3$ views, the joint training approach provides competitive results to using all N views, and exceeds the reported performance in the original MVDet paper [17].

We present an example of the selected views in the Wildtrack dataset in Fig. 9.

5.3. Efficiency Analysis

In Table 4, following previous works in efficient inference [24, 18], we detail the computational cost in FLOPs for task networks and MVSelect. Specifically, we find feature extraction $f(\cdot)$ to take up the majority of the computation, while everything else is lighter by at least an order of magnitude. Overall, we verify that using $T = 2$ or 3 out of N views can reduce the computational cost to roughly T/N .

In terms of inference speed, we find reduction in FLOPs results in monotonically increasing throughputs, ranging from $1.72\times$ to $3.03\times$. Due to factors such as implementation, parallelization, and hardware limitations, actual speedups cannot actually reach the level of computational cost reduction, as suggested by previous study [28].

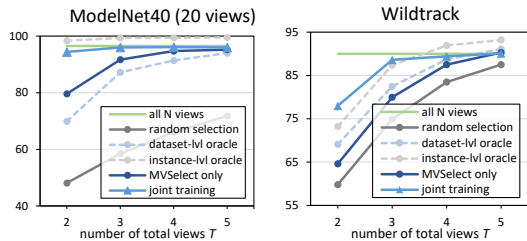


Figure 11: System performance under different number of total views T . We report classification accuracy and MODA for the two tasks, respectively (same for Fig. 12 and Table. 5). Circle and triangle markers indicate whether the task network is fixed or not, respectively. Dotted lines represent oracle performance (not achievable).

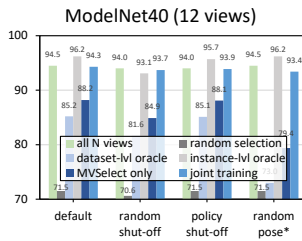


Figure 12: System evaluation under different settings. Except for the random pose* setting (where MVSelect variants are re-trained), all models are trained on the default setting.

5.4. Variant Study

Influence of total view count. The performance curves in Fig. 11 demonstrate that the joint training variant achieves competitive performance with as few as $T = 2$ views for multiview classification and $T = 3$ views for multiview detection, beyond which point performance plateaus. By contrast, learning MVSelect for fixed task networks shows a less steep curve. Notably, both datasets exhibit an increase in performance up to a total of $T = 5$ views, at which point the MVSelect policy performs comparably to the full N -view system.

Camera layout optimization. Determining the optimal camera locations is crucial for setting up an effective multiview system. In Fig. 8, we observe that not all cameras are equally useful according to the MVSelect policy. To address this, we allocate a validation partition of the data to identify the more useful camera views and then disable half of the $N = 12$ cameras that are not frequently utilized. In testing, we find that this new camera layout (policy shut-off” in Fig. 12) does not significantly impact the task network or the MVSelect module, and outperforms randomly disabling 6 of the 12 cameras (random shut-off” in Fig. 12). Although it is necessary to set up all N cameras for the analysis, optimizing the multiview camera layout can be a crucial step towards achieving optimal performance, and merits further investigation.

Random object pose. In real-world applications of multiview systems, such as those found in iPhones and Teslas, the cameras may remain fixed in their relative positions while the entire system is in motion. To simulate this scenario in our experiments, we introduce the random object pose setting (Fig. 12) and re-train MVSelect. While there is no exact object pose as supervision, the reinforcement learning approach is able to roughly infer the relative poses between the object and the multiview system, resulting in

improved performance compared to random selection and dataset-level oracle (which is arguably inappropriate for this setup). In the future, we plan to investigate the use of relative poses between multiview systems and the environment as supervision for moving system setups.

Ablation study. Regarding the MVSelect architecture design, Table 5 shows that removing the camera branch results in a MODA drop for the Wildtrack dataset, while the classification accuracy on ModelNet40 is not affected. Removing the feature branch brings the classification accuracy to dataset-level oracle (Table 2), but it does not significantly affect the multiview classification results.

This aligns with the policy we learned for the two tasks. For multiview detection, since the system has no clue about areas outside camera FoVs, MVSelect tends to guess and choose cameras that provide the overall best results. Therefore, the camera branch plays a more important role, as it encodes prior knowledge based on the initial camera. For multiview classification, however, target objects are fully observable, and MVSelect can make different decisions for each instance. In this case, the feature branch is more important, as it enables per-instance decision making.

6. Conclusion

In conclusion, this paper proposes an efficient approach for multiview systems by leveraging the camera layout and limiting the number of views. Through the use of a camera view selection module, MVSelect, jointly trained with the task network using reinforcement learning, the proposed approach demonstrates competitive performance on multiview classification and detection tasks at fractions of the computational cost. Overall, the proposed efficient approach provides an alternative to reducing image resolution and using lighter networks, and paves way for future multiview camera layout optimization.

	views	FLOPs			throughput
		$f(\cdot)$	$g(\cdot)$	$d(\cdot)$	(instance/s)
ModelNet40	20	36.5G	20.5k	N/A	119.6
	2	3.6G	20.5k	1.1M	361.8
	12	21.9G	20.5k	N/A	196.2
Wildtrack	2	3.6G	20.5k	530.4k	507.9
	7	1.2T	19.1G	N/A	8.4
MultiviewX	3	511.6G	19.1G	3.2G	16.2
	6	1.0T	17.7G	N/A	9.8
	3	511.6G	17.7G	2.9G	16.9

Table 4: Computational cost and speed.

	ModelNet40 12 views	Wildtrack
MVSelect only	88.2	80.0
w/o camera branch	88.2	79.1
w/o feature branch	85.0	79.9

Table 5: Ablation study.

References

- [1] John Aloimonos, Isaac Weiss, and Amit Bandyopadhyay. Active vision. *International journal of computer vision*, 1:333–356, 1988. 1, 2
- [2] Peter Anderson, Qi Wu, Damien Teney, Jake Bruce, Mark Johnson, Niko Sünderhauf, Ian Reid, Stephen Gould, and Anton Van Den Hengel. Vision-and-language navigation: Interpreting visually-grounded navigation instructions in real environments. In *Proceedings of the IEEE conference on computer vision and pattern recognition*, pages 3674–3683, 2018. 3
- [3] Apple. iphone 14 pro and iphone 14 pro max. <https://www.apple.com/iphone-14-pro/>. 1, 2
- [4] Pierre Baqué, François Fleuret, and Pascal Fua. Deep occlusion reasoning for multi-camera multi-target detection. In *Proceedings of the IEEE International Conference on Computer Vision*, pages 271–279, 2017. 2, 6
- [5] Tatjana Chavdarova, Pierre Baqué, Stéphane Bouquet, Andrii Maksai, Cijo Jose, Timur Bagautdinov, Louis Lettry, Pascal Fua, Luc Van Gool, and François Fleuret. Wild-track: A multi-camera hd dataset for dense unscripted pedestrian detection. In *Proceedings of the IEEE Conference on Computer Vision and Pattern Recognition*, pages 5030–5039, 2018. 1, 5, 6, 7
- [6] Tatjana Chavdarova et al. Deep multi-camera people detection. In *2017 16th IEEE International Conference on Machine Learning and Applications (ICMLA)*, pages 848–853. IEEE, 2017. 2, 6
- [7] Shengyong Chen, Youfu Li, and Ngai Ming Kwok. Active vision in robotic systems: A survey of recent developments. *The International Journal of Robotics Research*, 30(11):1343–1377, 2011. 1, 2
- [8] Alexey Dosovitskiy, Lucas Beyer, Alexander Kolesnikov, Dirk Weissenborn, Xiaohua Zhai, Thomas Unterthiner, Mostafa Dehghani, Matthias Minderer, Georg Heigold, Sylvain Gelly, Jakob Uszkoreit, and Neil Houlsby. An image is worth 16x16 words: Transformers for image recognition at scale. *ICLR*, 2021. 1
- [9] ABI Research: The Tech Intelligence Experts. More than 155,000 smart ai-based cameras will transform traffic management by 2025. <https://www.abiresearch.com/press/more-155000-smart-ai-based-cameras-will-transform-traffic-management-2025/>. 1
- [10] Yifan Feng, Zizhao Zhang, Xibin Zhao, Rongrong Ji, and Yue Gao. Gvcnn: Group-view convolutional neural networks for 3d shape recognition. In *Proceedings of the IEEE conference on computer vision and pattern recognition*, pages 264–272, 2018. 2, 3, 6
- [11] John M Findlay and Iain D Gilchrist. *Active vision: The psychology of looking and seeing*. Number 37. Oxford University Press, 2003. 1, 2
- [12] Francois Fleuret, Jerome Berclaz, Richard Lengagne, and Pascal Fua. Multicamera people tracking with a probabilistic occupancy map. *IEEE transactions on pattern analysis and machine intelligence*, 30(2):267–282, 2007. 2, 6
- [13] Xin Gao, Yijin Xiong, Guoying Zhang, Hui Deng, and Kangkang Kou. Exploiting key points supervision and grouped feature fusion for multiview pedestrian detection. *Pattern Recognition*, 131:108866, 2022. 3
- [14] Abdullah Hamdi, Silvio Giancola, and Bernard Ghanem. Mvtn: Multi-view transformation network for 3d shape recognition. In *Proceedings of the IEEE/CVF International Conference on Computer Vision*, pages 1–11, 2021. 2, 3, 5, 6
- [15] Kaiming He, Xiangyu Zhang, Shaoqing Ren, and Jian Sun. Deep residual learning for image recognition. In *Proceedings of the IEEE conference on computer vision and pattern recognition*, pages 770–778, 2016. 1, 6
- [16] Yunzhong Hou and Liang Zheng. Multiview detection with shadow transformer (and view-coherent data augmentation). In *Proceedings of the 29th ACM International Conference on Multimedia*, pages 1673–1682, 2021. 2, 3, 6
- [17] Yunzhong Hou, Liang Zheng, and Stephen Gould. Multiview detection with feature perspective transformation. In *Euro-pean Conference on Computer Vision*, pages 1–18. Springer, 2020. 1, 2, 3, 5, 6, 7
- [18] Andrew G Howard, Menglong Zhu, Bo Chen, Dmitry Kalenichenko, Weijun Wang, Tobias Weyand, Marco Andreetto, and Hartwig Adam. Mobilenets: Efficient convolutional neural networks for mobile vision applications. *arXiv preprint arXiv:1704.04861*, 2017. 1, 7
- [19] Jinwoo Hwang, Philipp Benz, and Tae-hoon Kim. Boostershot: Boosting stacked homography transformations for multiview pedestrian detection with attention. *arXiv preprint arXiv:2208.09211*, 2022. 3
- [20] Asako Kanezaki, Yasuyuki Matsushita, and Yoshifumi Nishida. Rotationnet: Joint object categorization and pose estimation using multiviews from unsupervised viewpoints. In *Proceedings of the IEEE conference on computer vision and pattern recognition*, pages 5010–5019, 2018. 1, 2, 3, 5, 6
- [21] Rangachar Kasturi, Dmitry Goldgof, Padmanabhan Soundararajan, Vasant Manohar, John Garofolo, Rachel Bowers, Matthew Boonstra, Valentina Korzhova, and Jing Zhang. Framework for performance evaluation of face, text, and vehicle detection and tracking in video: Data, metrics, and protocol. *IEEE Transactions on Pattern Analysis and Machine Intelligence*, 31(2):319–336, 2008. 5
- [22] Diederik P Kingma and Jimmy Ba. Adam: A method for stochastic optimization. In *ICLR (Poster)*, 2015. 6
- [23] Thomas N Kipf and Max Welling. Semi-supervised classification with graph convolutional networks. In *J. International Conference on Learning Representations (ICLR 2017)*, 2016. 2
- [24] Hao Li, Asim Kadav, Igor Durdanovic, Hanan Samet, and Hans Peter Graf. Pruning filters for efficient convnets. In *International Conference on Learning Representations*, 2017. 7
- [25] João Paulo Lima, Rafael Roberto, Lucas Figueiredo, Francisco Simões, Diego Thomas, Hideaki Uchiyama, and Veronica Teichrieb. 3d pedestrian localization using multiple cameras: a generalizable approach. *Machine Vision and Applications*, 33(4):1–16, 2022. 3

- [26] Volodymyr Mnih, Nicolas Heess, Alex Graves, et al. Recurrent models of visual attention. *Advances in neural information processing systems*, 27, 2014. 2, 3
- [27] Volodymyr Mnih, Koray Kavukcuoglu, David Silver, Alex Graves, Ioannis Antonoglou, Daan Wierstra, and Martin Riedmiller. Playing atari with deep reinforcement learning. *arXiv preprint arXiv:1312.5602*, 2013. 3
- [28] Pavlo Molchanov, Stephen Tyree, Tero Karras, Timo Aila, and Jan Kautz. Pruning convolutional neural networks for resource efficient inference. *arXiv preprint arXiv:1611.06440*, 2016. 1, 7
- [29] University of Parma and University of Pavia. The argo project. http://www.argo.ce.unipr.it/ARGO/english/flyer_en.pdf. 1
- [30] Charles R Qi, Hao Su, Matthias Nießner, Angela Dai, Mengyuan Yan, and Leonidas J Guibas. Volumetric and multi-view cnns for object classification on 3d data. In *Proceedings of the IEEE conference on computer vision and pattern recognition*, pages 5648–5656, 2016. 1, 2, 3, 5
- [31] Rui Qiu, Ming Xu, Yuyao Yan, Jeremy S Smith, and Xi Yang. 3d random occlusion and multi-layer projection for deep multi-camera pedestrian localization. *arXiv preprint arXiv:2207.10895*, 2022. 2, 3
- [32] Gemma Roig, Xavier Boix, Horesh Ben Shitrit, and Pascal Fua. Conditional random fields for multi-camera object detection. In *2011 International Conference on Computer Vision*, pages 563–570. IEEE, 2011. 2
- [33] Carl F Sabottke and Bradley M Spieler. The effect of image resolution on deep learning in radiography. *Radiology. Artificial intelligence*, 2(1), 2020. 1
- [34] John Schulman, Nicolas Heess, Theophane Weber, and Pieter Abbeel. Gradient estimation using stochastic computation graphs. *Advances in neural information processing systems*, 28, 2015. 3
- [35] John Schulman, Filip Wolski, Prafulla Dhariwal, Alec Radford, and Oleg Klimov. Proximal policy optimization algorithms. *arXiv preprint arXiv:1707.06347*, 2017. 3
- [36] Jacob Shermeyer and Adam Van Etten. The effects of super-resolution on object detection performance in satellite imagery. In *Proceedings of the IEEE/CVF Conference on Computer Vision and Pattern Recognition Workshops*, pages 0–0, 2019. 1
- [37] Liangchen Song, Jialian Wu, Ming Yang, Qian Zhang, Yuan Li, and Junsong Yuan. Stacked homography transformations for multi-view pedestrian detection. In *Proceedings of the IEEE/CVF International Conference on Computer Vision*, pages 6049–6057, 2021. 2, 3, 6
- [38] Hang Su, Subhransu Maji, Evangelos Kalogerakis, and Erik Learned-Miller. Multi-view convolutional neural networks for 3d shape recognition. In *Proceedings of the IEEE international conference on computer vision*, pages 945–953, 2015. 1, 2, 3, 5, 6, 7
- [39] Richard S Sutton and Andrew G Barto. *Reinforcement learning: An introduction*. MIT press, 2018. 5
- [40] Unity Technologies. Unity. <https://unity.com/>. 5
- [41] Tesla. Model 3 owner’s manual. https://www.tesla.com/ownersmanual/model3/en_us/GUID-EDA77281-42DC-4618-98A9-CC62378E0EC2.html. 1, 2
- [42] Jeet Vora, Swetanjali Dutta, Kanishk Jain, Shyamgopal Karthik, and Vineet Gandhi. Bringing generalization to deep multi-view detection. *arXiv preprint arXiv:2109.12227*, 2021. 2, 3
- [43] Chu Wang, Marcello Pelillo, and Kaleem Siddiqi. Dominant set clustering and pooling for multi-view 3d object recognition. *arXiv preprint arXiv:1906.01592*, 2019. 3
- [44] Xin Wei, Ruixuan Yu, and Jian Sun. View-gcn: View-based graph convolutional network for 3d shape analysis. In *Proceedings of the IEEE/CVF Conference on Computer Vision and Pattern Recognition*, pages 1850–1859, 2020. 2, 3, 5, 6
- [45] Ronald J Williams. Simple statistical gradient-following algorithms for connectionist reinforcement learning. *Reinforcement learning*, pages 5–32, 1992. 3
- [46] Zhirong Wu, Shuran Song, Aditya Khosla, Fisher Yu, Linguang Zhang, Xiaoou Tang, and Jianxiong Xiao. 3d shapenets: A deep representation for volumetric shapes. In *Proceedings of the IEEE conference on computer vision and pattern recognition*, pages 1912–1920, 2015. 1, 5, 6, 7
- [47] Yuanlu Xu, Xiaobai Liu, Yang Liu, and Song-Chun Zhu. Multi-view people tracking via hierarchical trajectory composition. In *Proceedings of the IEEE Conference on Computer Vision and Pattern Recognition*, pages 4256–4265, 2016. 2, 6
- [48] Ze Yang and Liwei Wang. Learning relationships for multi-view 3d object recognition. In *Proceedings of the IEEE/CVF International Conference on Computer Vision*, pages 7505–7514, 2019. 3, 5, 6
- [49] Tan Yu, Jingjing Meng, and Junsong Yuan. Multi-view harmonized bilinear network for 3d object recognition. In *Proceedings of the IEEE conference on computer vision and pattern recognition*, pages 186–194, 2018. 3, 5, 6
- [50] Yuke Zhu, Roozbeh Mottaghi, Eric Kolve, Joseph J Lim, Abhinav Gupta, Li Fei-Fei, and Ali Farhadi. Target-driven visual navigation in indoor scenes using deep reinforcement learning. In *2017 IEEE international conference on robotics and automation (ICRA)*, pages 3357–3364. IEEE, 2017. 3